Journal of Alloys and Compounds 498 (2010) 95–101

Contents lists available at ScienceDirect

Journal of Alloys and Compounds

journal homepage: www.elsevier.com/locate/jallcom

Microstructure, mechanical properties, hot deformation and oxidation behavior of Ti–45Al–5.4V–3.6Nb–0.3Y alloy

Y.Y. Chen[a], F. Yang[a,b,*], F.T. Kong[a], S.L. Xiao[a]

[a] School of Materials Science and Engineering, Harbin Institute of Technology, Harbin 150001, PR China
[b] Department of Powder Metallurgy, Guangzhou Research Institute of Non-ferrous Metal, Guangzhou 510651, PR China

ARTICLE INFO

Article history:
Received 31 October 2009
Received in revised form 10 March 2010
Accepted 13 March 2010
Available online 19 March 2010

Keywords:
TiAl alloy
Microstructure and properties
Deformability
Oxidation

ABSTRACT

γ-TiAl alloys are regarded as promising structural materials for extensively using in the fields of aerospace, automobile vehicle and chemistry. In this paper, microstructure, properties and hot deformation behavior of Ti–45Al–5.4V–3.6Nb–0.3Y alloy were investigated. SEM, XRD and TEM results showed that the alloy mainly composed of γ, α_2 and β phase had fine nearly lamellar microstructure with colony size of 50–70 μm, β and γ phase located at the colony boundaries. In addition, some β precipitations appeared at γ/γ interfaces. Tensile test results exhibited that the yield strength (YS) and ultimate tensile strength (UTS) of the alloy were decreased from 400 MPa and 460 MPa at room temperature to 350 MPa and 420 MPa at 700 °C, respectively, and the elongation (δ) of the alloy was increased from 0.55% at room temperature to 2.63% at 700 °C. The fracture surfaces exhibited primary translamellar character at all test temperatures. Ti–45Al–5.4V–3.6Nb–0.3Y alloy showed excellent deformability at elevated temperature since some β phases exist at the colony boundaries. At 800 °C, the alloy owned a good oxidation resistance due to the presence of an almost fully dense oxidation layer with an alternating structure which formed during oxidation processing.

1. Introduction

TiAl based alloys are very promising materials due to their combination properties of low density, high specific strength, high specific stiffness, good creep strength up to 700 °C, and better high temperature oxidation resistance than titanium alloys, which are attractive for use in advanced propulsion systems for aircraft and also in automobile engine parts [1–3]. However, the low room temperature ductility and poor formability limit the extensive application of TiAl based alloys [4]. During last decades, considerable efforts have been devoted to improve the both room temperature ductility and formability, and some typical TiAl alloys and components were produced through optimizing of alloy composition and processing routs. For example, Clemens et al developed γ-TAB (Ti–47Al–4(Cr, Mn, Nb, Si, B)), γ-Met (Ti–46.5Al–4(Cr, Nb, Ta, B)) and γ-TNB [5,6] alloys, these alloys had fine grain size of about 5–8 μm. Gerling et al. have successfully manufactured Ti–45Al–5Nb(0,0.5)C sheets by hot rolling of PM pre-materials [7]. Tetsui et al. [8,9] used the conventional hot-working technique to prepare structural components of TiAl based alloys.

Recently, Kim et al. put forward a new concept of beta γ-TiAl alloys which solidified through the beta-solidification process. Such alloys were determined to exist experimentally within a broad composition range of Ti–(40–45)Al–(2–7)Nb–(1–9)(Cr, Mn, V, Mo)–(0–0.5)(B, C) [10]. They exhibited excellent formability above 1100 °C due to the existence of β(B2) phase. In this paper, a new beta γ-TiAl alloy with a nominal composition of Ti–45Al–5.4V–3.6Nb–0.3Y alloy has been prepared and microstructure, mechanical properties, hot deformation and oxidation behavior were studied.

2. Experimental procedure

The ingot with a composition of Ti–45Al–5.4V–3.6Nb–0.3Y was prepared by arc-melting under a high-purity argon gas environment using non-consumable electrode. The parent materials used in this study contained sponge Ti, high-purity Al, Al–V, Al–Nb and Al–Y interalloys, and the melting cycle was repeated at least five times to obtain homogenous button ingot. Subsequently, the ingot was treated by a heat treatment (900 °C, 72 h) in air to eliminate the residual stress and reduce the composition segregation.

For the as-cast materials, tensile tests were conducted at room temperature and 700 °C in air on an Instron testing machine at a strain rate of 5×10^{-4} s^{-1}. The hot compressive test with sample size of Ø8 mm × 12 mm was carried out at 1200 °C on a Gleeble 1500D thermal simulating machine at a strain of 10^{-2} s^{-1} and deformation of 60%. For the oxidation test, the samples were cut into rectangular samples with a dimension of 8 mm × 6 mm × 4 mm, and their surfaces were polished with 600# SiC papers, cleaned in acetone and ethanol, and then measured and weighted. Cyclic oxidation test was conducted at 800 °C in static air for 80 h.

* Corresponding author at: P.O. Box 434, Harbin Institute of Technology, Harbin 150001, PR China. Tel.: +86 451 86418802; fax: +86 451 86418802.
E-mail address: fyang0204@hotmail.com (F. Yang).

0925-8388/$ – see front matter © 2010 Elsevier B.V. All rights reserved.
doi:10.1016/j.jallcom.2010.03.118

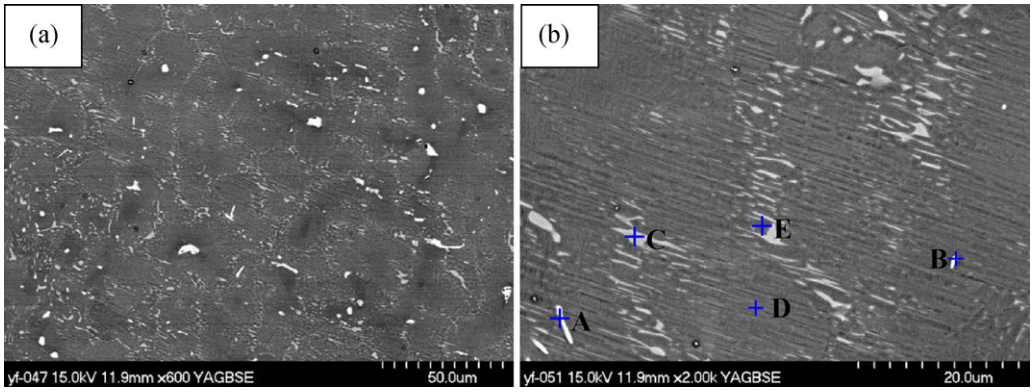

Fig. 1. Microstructures of Ti–45Al–5.4V–3.6Nb–0.3Y: (a) BSE image and (b) BSE image in large visual field.

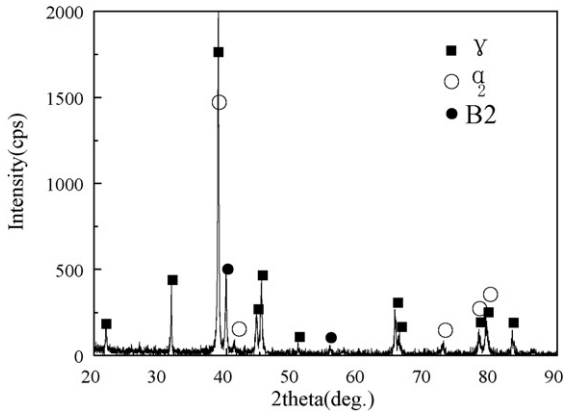

Fig. 2. XRD pattern of Ti–45Al–5.4V–3.6Nb–0.3Y alloy.

Microstructures, oxidation scale and phase constitution were analyzed via scanning electron microscopy (SEM), transmission electron microscopy (TEM) and X-ray diffraction (XRD), respectively. Samples were made by wire cutting from the ingot, the polished surface for SEM was etched in a modified Kroll's reagent of 10 vol.% HF, 4 vol.% HNO_3 and 86 vol.% H_2O. Samples for TEM observation were prepared using twin-jet electropolishing method in a solution of 60 vol.% methanol, 34 vol.% normal butanol and 6 vol.% perchloric acid at −20 °C and a potential of 40 V. XRD analysis of this alloy was carried out via Cu Kα radiation (λ = 0.154157 nm) and 2θ from 20° to 120°.

3. Results and discussion

3.1. Microstructure of Ti–45Al–5.4V–3.6Nb–0.3Y alloy

As shown in Fig. 1, the Ti–45Al–5.4V–3.6Nb–0.3Y alloy shows homogenous, fine-grained nearly lamellar structure, and the lamellar colony size is about 50–70 μm. The columnar character is much less pronounced compared to conventional TiAl alloy [11]. There is evidence of the γ phase and β(B2) phase along lamellar colony boundaries (Fig. 1a). X-ray diffraction pattern shows the phase constitution of Ti–45Al–5.4V–3.6Nb–0.3Y alloy (Fig. 2), and the results confirm that the alloy primarily consists of the γ phase besides a small amount of β(B2) and α_2 phases. In order to further investigate the distribution and constitution of different phases, more details are presented in a larger visual field in BSE mode (Fig. 1b). EDS results taken from the different phases in Fig. 1b are summarized in Table 1. The bright particle A is enriched in element Y and Al with the ratio of nearly 2:1 and element Ti and V are at low levels in this particle. The particle can be determined as the YAl_2 phase which can impede the growth of grain according to the previous research [12]. The average composition of element Y and O in particle B is 40.01 at.% and 43.39 at.%, respectively, thus this particle can be regarded as Y_2O_3 phase. The existence of Y_2O_3 phase can purify the Ti–45Al–5.4V–3.6Nb–0.3Y alloy, which is attributed to high affinity of Y and O. The YAl_2 and Y_2O_3 phase are absent in XRD pattern, and the reason is that the amount is too low to be detected by XRD. The grey β(B2) phase (particle C) has the average compositions of 47.43Ti, 36.80Al, 10.45V and 5.31Nb (at.%). The lamellar structure (position D) and dark single γ phase (position E) have the average compositions of 48.18Ti, 42.99Al, 4.82V, 3.82Nb, 0.18Y (at.%) and 46.31Ti, 46.05Al, 4.20V, 3.24Nb, 0.20Y (at.%), respectively. It should be noted that V and Nb concentration are obvious different in the different phases. Relatively high V and Nb concentration in the β phase is consistent with the viewpoint that V and Nb can stabilize the β phase in TiAl alloys [11,13]. The V and Nb concentration in lamellae are about 4.82% and 3.82%, respectively, which are slightly higher than that in γ phase.

Fig. 3 shows the lamellar structure of Ti–45Al–5.4V–3.6Nb–0.3Y alloy. It can be seen that some precipitates appear within the lamellar structure besides the γ and α_2 lamellae. These precipitates are identified as β(B2) phase with bcc structure ($a \approx 0.316$ nm), as shown in Fig. 3b. The precipitated β(B2) particles exist at the γ/γ interface, which is strong evidence that the decisive factor to form the β phase is the supersaturation of V and Nb in the γ plates. Usually, the transformation allows the following relationship between β and γ phase: $\{1\,1\,0\}_\beta // \{1\,1\,1\}_\gamma$ and $\langle 1\,1\,1\rangle_\beta // \langle 1\,1\,0\rangle_\gamma$ [14].

It is well known that V and Nb are β stabilizer, and the solidification mode of TiAl alloys will be promoted to shift from α-solidification to β-solidification after adding such elements [11,13]. The alloys solidified through β phase show much less obvious columnar character, the reason is that the ⟨1 0 0⟩ axis of β phase is the preferential direction of crystal growth during solidification. There are three equivalent directions for bcc β phase ⟨1 0 0⟩ orientation, which are [1 0 0], [0 1 0] and [0 0 1]. This is very different from α-solidification where there is only one orientation (the *c*-axis) for preferential crystal growth. Therefore, the microstructure of Ti–45Al–5.4V–3.6Nb–0.3Y alloy exhibits much more pronounced equiaxed character than the columnar character.

According to the phase diagram presented by Takeyama and Kobayashi [15], the equilibrium solidification route of the Ti–45Al–*x*V alloy is as following: $L \rightarrow \beta \rightarrow \alpha+\beta \rightarrow \alpha \rightarrow \alpha+\beta \rightarrow \alpha+\beta+\gamma \rightarrow \beta+\gamma$, and the equilibrium microstructure should be β + γ structure. However, the microstructure of Ti–45Al–5.4V–3.6Nb–0.3Y alloy exhibit the evidence of the following solidification and transformation path way: $L \rightarrow L+\beta \rightarrow \beta \rightarrow \alpha+\beta \rightarrow \alpha+\beta+\gamma \rightarrow$ Lamellar + β + γ. The β phase is stabilized by high V and Nb addition. During the cooling, the $\beta \rightarrow \alpha$ transformation is incomplete due to the stability of the β phase and the high cooling rate. The lamellar structure is transformed from high temperature α phase. At the same time, the β + γ structure is formed as the γ phase precipitates from

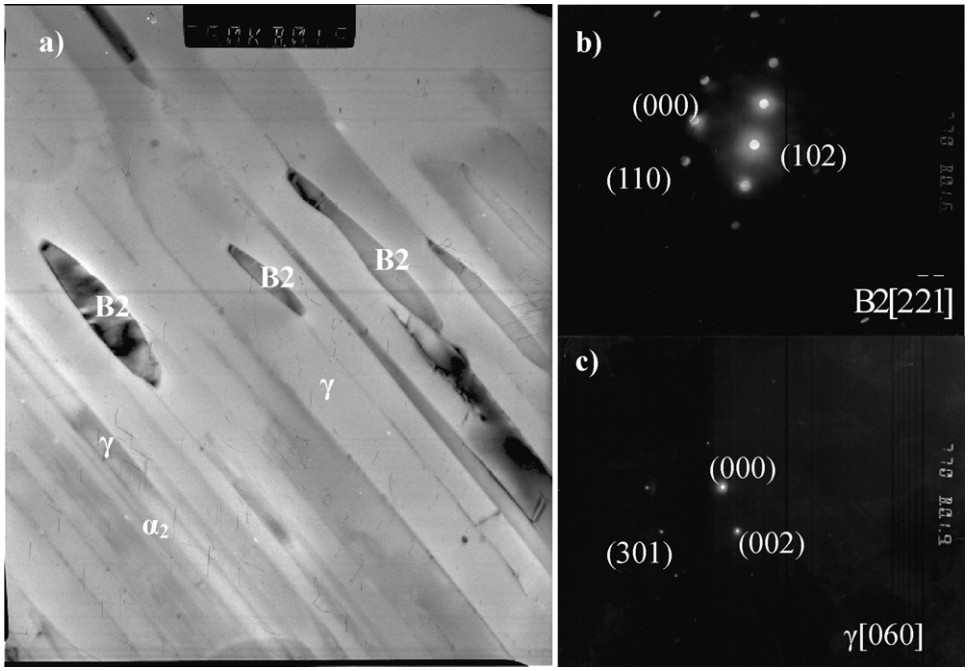

Fig. 3. Lamellar structure of Ti–45Al–5.4V–3.6Nb–0.3Y alloy: (a) TEM image of γ, α2 and β precipitates, (b) the diffraction pattern of β precipitates and (c) the diffraction pattern of γ phase.

high temperature β or α phase [14]. The resultant microstructure of Ti–45Al–5.4V–3.6Nb–0.3Y alloy is characterized by the nearly lamellar colonies surrounded by β and γ phase. This type of microstructure is helpful for improving the hot deformability of Ti–45Al–5.4V–3.6Nb–0.3Y alloy, and the reason will be discussed in the following sections.

3.2. Mechanical properties and fracture behavior

Fig. 4 shows the tensile properties of Ti–45Al–5.4V–3.6Nb–0.3Y alloy at RT and 700 °C. It is apparent that the alloy has a moderate strength and ductility at room and elevated temperature. At room temperature, the YS and UTS are about 400 MPa and 460 MPa, respectively, and the δ is about 0.55%. With increasing of the temperature to 700 °C, the YS and UTS are decreased to 350 MPa and 420 MPa, and the δ is increased to 2.63%, respectively. As shown in Fig. 5, the Ti–45Al–5.4V–3.6Nb–0.3Y alloy has a brittle and translamellar fracture mode, hinting that the crack spread parallel or perpendicular to the lamellar interfaces. No intergranular cracks and dimples are observed. It is also noted that the test temperature has little effect on fracture mode.

The Ti–45Al–5.4V–3.6Nb–0.3Y alloy has moderate mechanical properties at room temperature and 700 °C. This is mainly attributed to the fine colony size, which benefits both strength and ductility. Furthermore, it is generally believed [16] that the primary slip systems in TiAl alloy are ⟨0 1 1⟩{1 1 1} ordinary dislocation which can be activated at low temperature and 1/2⟨1 1 0]{1 1 1} dislocations which are related to high temperature deformation. However, V additions may cause the high temperature 1/2⟨1 1 0] slip system to be partly extended to low temperatures, this is beneficial for ductility of Ti–45Al–5.4V–0.3Y alloy at room temperature. In addition, the addition of Y can react with O during solidification and the Y_2O_3 phase forms, so that the content of oxygen in the alloy is lowered and the TiAl alloy is purified. This may also enhance the mobility of 1/2⟨1 1 0]{1 1 1} dislocations at room temperature [17]. In other words, the existence of Y_2O_3, to some extent, also can improve the ductility of Ti–45Al–5.4V–3.6Nb–0.3Y alloy.

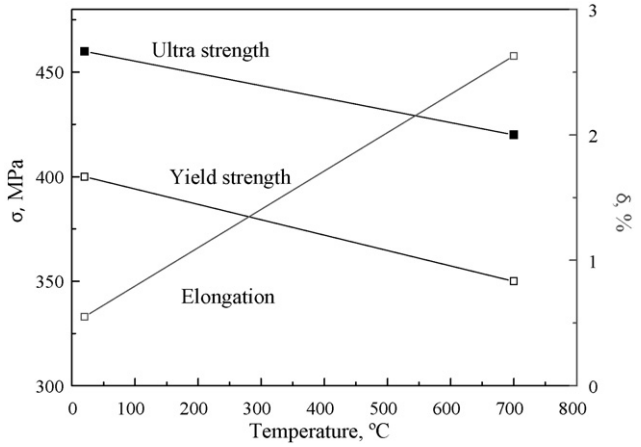

Fig. 4. Mechanical properties of Ti–45Al–5.4V–3.6Nb–0.3Y alloy.

Table 1
Chemical composition of different positions of Ti–45Al–5.4V–3.6Nb–0.3Y alloy.

Position	Ti (at.%)	Al (at.%)	V (at.%)	Nb (at.%)	Y (at.%)	O (at.%)
A	15.61	58.75	01.46	01.03	23.16	0
B	07.83	07.30	01.16	00.32	40.01	43.39
C	47.43	36.80	10.45	05.31	0	0
D	48.18	42.99	04.82	03.82	00.18	0
E	46.31	46.05	04.20	03.24	00.20	0

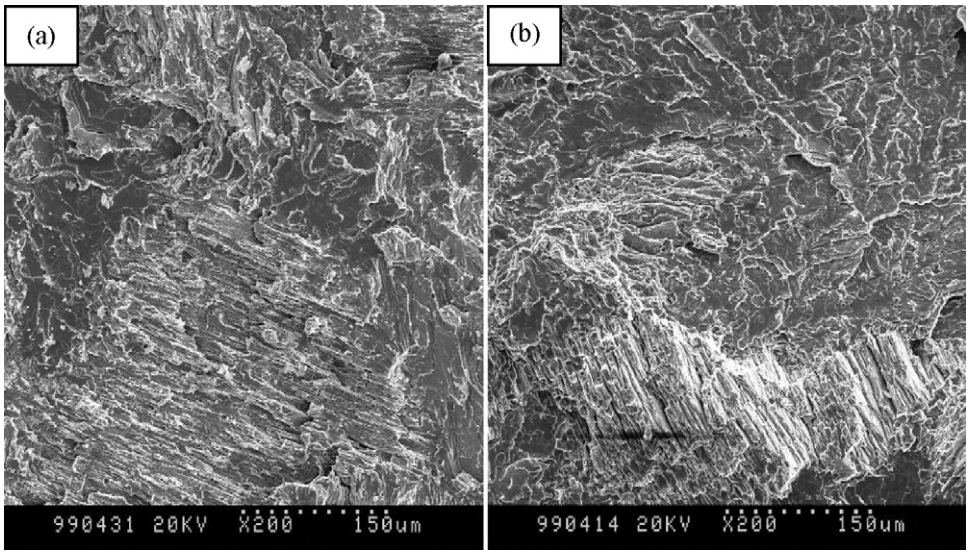

Fig. 5. Fracture surface of Ti–45Al–5.4V–3.6Nb–0.3Y alloy: (a) at room temperature and (b) at 700 °C.

Increasing test temperature from room temperature to 700 °C, the strength decreases and ductility increases. At elevated temperature, grain boundary sliding and mechanical twinning can become active, and more dislocation movements are feasible. In the meantime, the glide of 1/2⟨1 1 0] dislocations or twinning can introduce high constraint stresses by the shape change of adjacent grains, which are believed to assist superdislocations in overcoming the high lattice friction. Hence, the glide processes of these dislocations are locally initiated and the strain compatibility among different grains is improved during the deformation. As a result, the lower strength and higher ductility can be obtained at elevated temperature.

In lamellar TiAl alloys, micro-cracks generally initiate at γ/α_2 or γ/γ interfaces and propagate parallel or perpendicular to the interfaces. Cracking along the interfaces is detrimental, because the cracks can spread quickly throughout the whole lamellar colony once they are initiated. The likelihood of premature failure is exacerbated when the lamellar colony size is large. The critical crack length can be estimated using the equation [18]:

$$K1c = \sigma\sqrt{\pi a}$$

Here K_{1c} is fracture toughness, σ is fracture stress and a is a half of critical crack length. For TiAl alloys with a K_{1c} of about 20 MPa $m^{1/2}$ at a stress level of 460 MPa, the critical crack length is about 1204 μm. Moreover, it is difficult for cracks to cross the lamellar colony boundaries since they will be deflected due to the misorientation of the neighbouring colonies. Therefore, it indicates that Ti–45Al–5.4V–3.6Nb–0.3Y alloy with a fine colony size can limit the fast growth and spread of cracks.

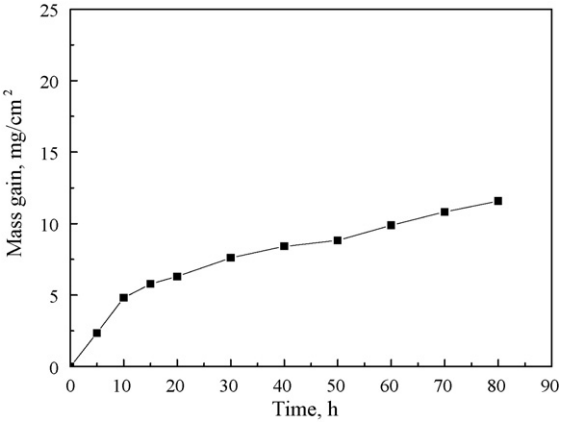

Fig. 7. Oxidation morphology of Ti–45Al–5.4V–3.6Nb–0.3Y alloy after cyclical oxidation test at 800 °C/80 h.

3.3. Hot deformation behavior

Fig. 6a shows the hot processing curve of Ti–45Al–5.4V–3.6Nb–0.3Y alloy at 1200 °C and a strain rate of 10^{-2} s^{-1} with deformation of 60%. As the degree of the deformation increases, the flow stress increase promptly to

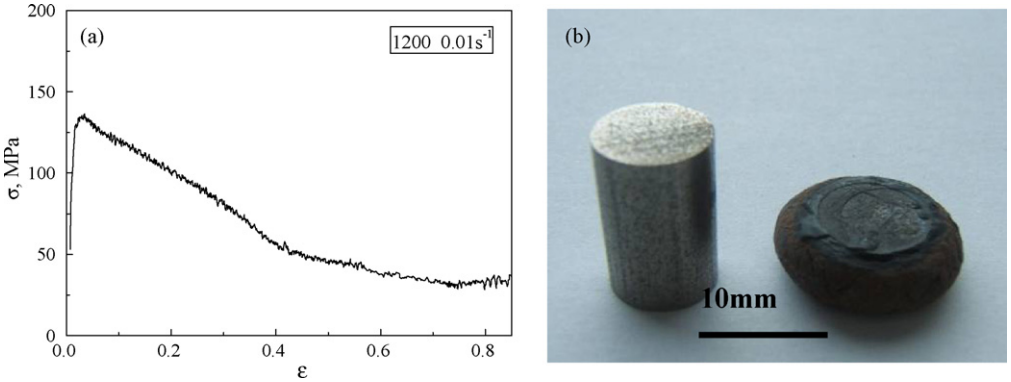

Fig. 6. Thermal simulating curve and deformed sample of Ti–45Al–5.4V–3.6Nb–0.3Y alloy at 1200 °C, 10^{-2} s^{-1}, 60%: (a) compressive curve and (b) deformed sample.

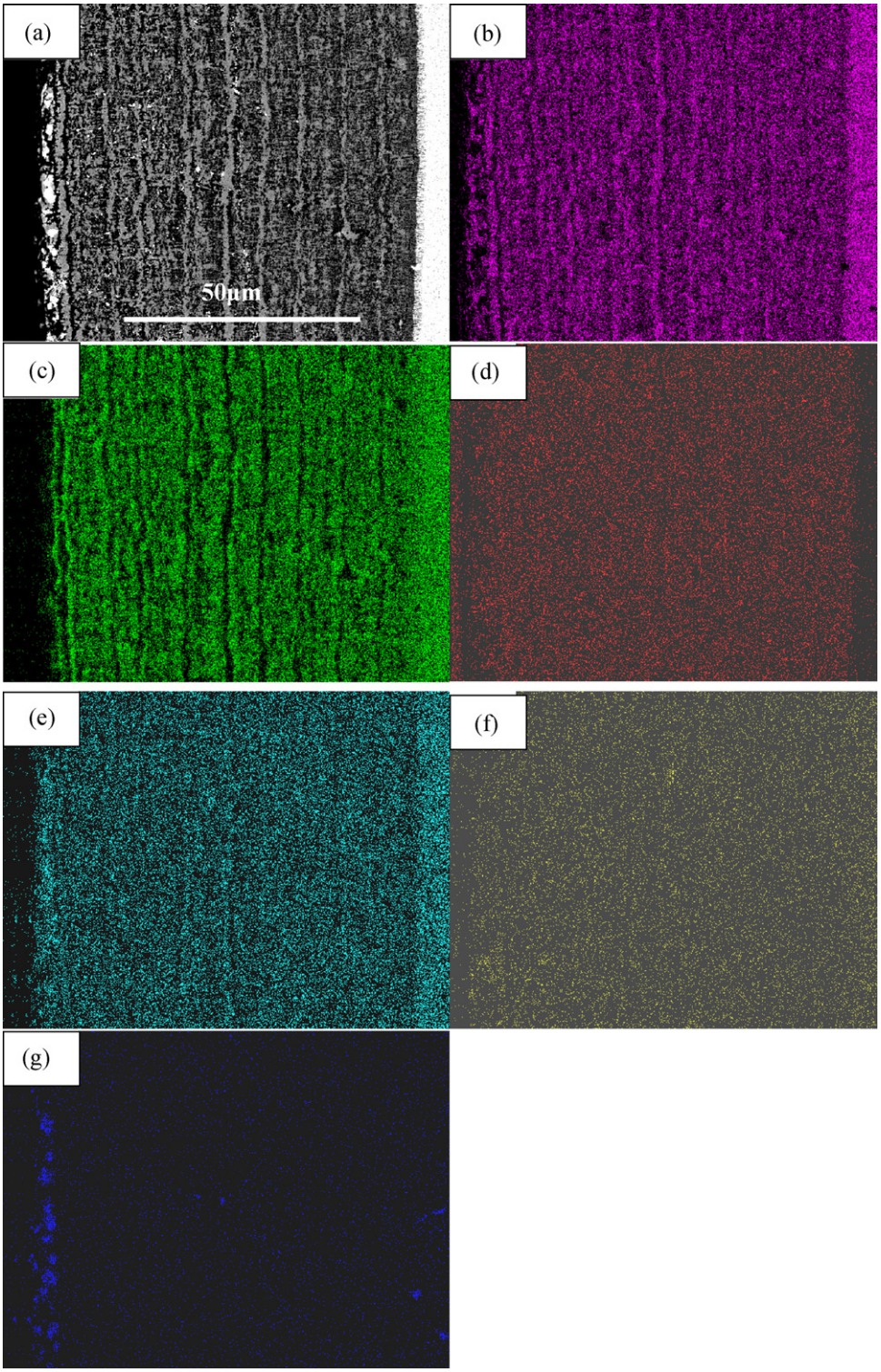

Fig. 8. Scale cross-section and element distribution maps in cross-section of Ti–45Al–5.4V–3.6Nb–0.3Y alloy after cyclical oxidation at 800 °C for 80 h: (a) scale, (b) Ti, (c) Al, (d) O, (e) V, (f) Nb and (g) Y.

the peak stress and then decrease quickly. Finally, a steady stage of flow is observed in the curve. The hot deformation process is related to work hardening and strain softening, a steady stage of flow indicates that a balance between work hardening and strain softening is achieved, this is favorable for deformation of Ti–45Al–5.4V–3.6Nb–0.3Y alloy and results in the sample not cracking after deforming, as shown in Fig. 6b.

Usually, investigators argue that the deformation of γ-TiAl at elevated temperature is related activity of ⟨1 1 0] ordinary dislocation [16,19], and ⟨0 1 0] dislocations may contribute to the deformation of TiAl alloy above 1000 °C [20]. Thus, under hot-working conditions the plastic anisotropy of γ(TiAl) is probably reduced and relatively large strains might be realized by the propagation of ordinary dislocations and twins. But this explanation is not adequate to explain the reason that the sample did not frac-

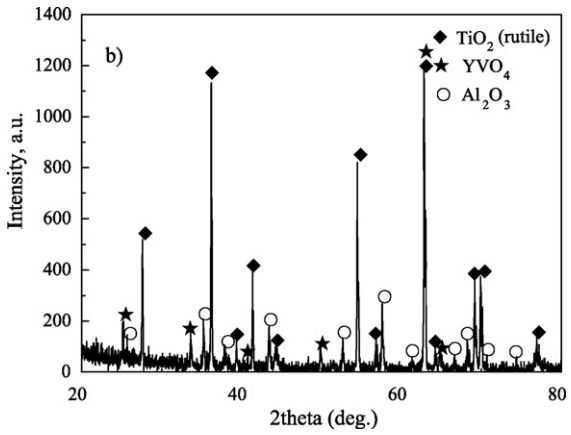

Fig. 9. XRD pattern of oxidation of Ti–45Al–5.4V–3.6Nb–0.3Y alloy after cyclical oxidation test at 800 °C/80 h.

ture with a large deformation of 60% in this research. As shown in Figs. 1b and 3a, some β(B2) phases locate at the lamellar colony boundaries and γ/γ interfaces in Ti–45Al–5.4V–3.6Nb–0.3Y alloy, which is probably beneficial for the hot deformation.

According to Takamaya's research, the B2 → β disordered transformation occurs above 1100 °C [14], and disordered β phase with a bcc structure offers more slip planes compared to the hexagonal α_2 phase and the tetragonal γ phase. Obviously, these slip systems are being activated at high temperature and this gives evidence that β phase shows excellent deformability compared to γ and α_2 phase. Therefore, the existence of β phase can enhance the deformability of Ti–45Al–5.4V–3.6Nb–0.3Y alloy at high temperature. In addition, grain boundary β phase acts like a lubricant which promotes grain boundary sliding and grain rotation during deformation [21], and Vanderschueren et al. [22] certify that the presence of β phase in TiAl alloy enhances the grain boundary cohesion, delays cavitation and fracture at high temperature. This further illustrates that the β phase in Ti–45Al–5.4V–3.6Nb–0.3Y alloy with nearly lamellar colonies and surrounded by β and γ phase is helpful for improving high temperature deformability of the alloy.

3.4. Oxidation

The curve of cyclic oxidation kinetics of the Ti–45Al–5.4V–3.6Nb–0.3Y alloy at 800 °C is shown in Fig. 7. The oxidation kinetics curve consists of two stages. In the early stage of oxidation (<10 h), the mass gain shows a linear relationship, indicating that the oxidation scale yielded in this stage is not protective for the alloy. After the initial period, the mass gain shows a parabolic increase. The overall mass gain and the scale thickness for Ti–45Al–5.4V–3.6Nb–0.3Y alloy upon cyclic oxidation for 80h exposure time are small, they are in order of 10 mg/cm^2 (Fig. 6) and 65 μm (as shown in Fig. 8a), respectively. In addition, a strip structure can be observed in the oxide scale of Ti–45Al–5.4V–3.6Nb–0.3Y alloy (Fig. 8a), to understand constitution of the strip structure, EDS analysis is carried out and the results (as shown in Fig. 8b–g) illustrate that the grey layers are rich in Ti and O elements, and dark layers abundant in Al and O elements. Elements Y, V and O are present in the bright particles of oxidation scale. Fig. 9 shows the XRD diffraction spectra of the oxide scale for Ti–45Al–5.4V–3.6Nb–0.3Y alloy after 80h exposure time at 800 °C. Basically, three different oxide phases of TiO_2, Al_2O_3 and YVO_4 are formed. Combining with EDS analysis, we can speculate that the strip structure are mainly composed of TiO_2 (grey layer) and Al_2O_3 (dark layer) phases, and the bright particles distributed in the strip structure is YVO_4 phase.

The poor oxidation resistance of TiAl alloys above 800 °C is due to the fact that they cannot form a long-lasting protective alumina scales [23,24]. One effective measure to improve the oxidation resistance of TiAl alloy is to promote the formation of a dense and alternating alumina scale through adding alloy elements, so that the diffusion of Ti^{4+} and O^{2-} can be impeded. For Ti–45Al–5.4V–3.6Nb–0.3Y alloy, several nearly dense and consecutive Al_2O_3 layers form in the oxidation scale during cyclic oxidation at 800 °C, which can ameliorate the oxidation resistance. According to the oxidation kinetics [24], the formation rate of Ti oxides is higher than that of alumina. Consequently, TiO_2 is preferentially formed in the external scale. The consumption of Ti promotes the activity of the Al underneath, moreover, the thermodynamic activity of Al relative to that of Ti is increased after adding Nb in the TiAl alloy and this favors the formation of stable alumina scale [25]. Accordingly, the Al_2O_3–rich phase forms in the inner layer. Then the formation of Al_2O_3–rich layer leads to Ti enrichment in the region beneath, and the TiO_2 rich region is formed again. Due to the alternating reaction of oxygen with Ti and Al, the inner scale eventually consist of strip structure which can impede the diffusion of Ti^{4+} and O^{2-} and decrease the oxidation rate of Ti–45Al–5.4V–3.6Nb–0.3Y alloy. Furthermore, TiO_2 can be doped by Nb in the TiAl alloy with addition of Nb, i.e., Nb^{5+} replace Ti^{4+}, leading to a decrease in oxygen vacancies. This slower diffusion of oxygen and growth rate of TiO_2 phase [26,27] has the benefit of improving oxidation resistance of Ti–45Al–5.4V–3.6Nb–0.3Y alloy. In addition, Nb can lower the solubility of oxygen in the alloy [28], thus restraining the internal oxidation of Ti–45Al–5.4V–3.6Nb–0.3Y alloy.

For elements Y and V, V is a deleterious element for oxidation behavior of TiAl alloy [29,30], and Y is a neutral element but Y addition can improve oxidation resistance of TiAl [31]. Li [32] investigated the oxidation behavior of TiAl alloy with V additions, and found that the poor oxidation of TiAl alloy with V additions was mainly attributed to yielding of V_2O_5 which is a volatile oxide. In Ti–45Al–5.4V–3.6Nb–0.3Y alloy, the stable oxide of YVO_4, reacted by Y_2O_3 and V_2O_5 [33], occurs in the oxidation scale and it can reduce the amount of V_2O_5 volatilizing and is beneficial for improving oxidation resistance of Ti–45Al–5.4V–3.6Nb–0.3Y.

4. Conclusions

Ti–45Al–5.4V–3.6Nb–0.3Y alloy is mainly composed of γ, α_2 and β phase besides a small amount of YAl_2 and Y_2O_3 phase. The alloy has a fine nearly lamellar microstructure with a lamellar colony size of 50–70 μm, and the β and γ phase locate at colony boundaries. Some β precipitates exist at the γ/γ interfaces, and the solidification and transformation path way is: $L \rightarrow L+\beta \rightarrow \beta \rightarrow \alpha+\beta \rightarrow \alpha+\beta+\gamma \rightarrow$ Lamellar + β + γ. The alloy exhibits moderate yield strength, fracture strength and ductility at room temperature and 700 °C, which are 400 MPa, 460 MPa and 0.55% at room temperature and 350 MPa, 420 MPa and 2.63% at 700 °C, respectively. The Ti–45Al–5.4V–3.6Nb–0.3Y alloy also exhibits excellent deformability at elevated temperature due to the introduction of β phase at the colony boundaries. During cyclic oxidation processing a nearly dense and alternating strip structure, composed of TiO_2 and Al_2O_3 phase, forms, reduces the oxidation rate and improves oxidation resistance of Ti–45Al–5.4V–3.6Nb–0.3Y alloy.

References

[1] M. Yamaguchi, H. Inui, K. Ito, Acta Mater. 48 (2000) 307–322.
[2] Y.W. Kim, JOM 7 (1994) 30–39.
[3] Y.W. Kim, JOM 7 (1989) 24–30.
[4] Y.W. Kim, D.M. Dimiduk, JOM 8 (1991) 40–47.
[5] R. Gerling, A. Bartels, H. Clemens, H. Kestler, F.P. Schimansky, Intermetallics 3 (2004) 275–280.

[6] H. Clemens, F. Appel, A. Bartels, H. Baur, R. Gerling, V. Guther, H. Kestler, in: G. Lutjeringand, J. Albrecht (Ed.), Ti-2003 Science and Technology, Germany, 2003, pp. 2123–2136.
[7] R. Gerling, F.P. Schimansky, A. Stark, A. Bartels, H. Kestler, L. Cha, C. Scheu, H. Clemens, Intermetallics 16 (2008) 689–697.
[8] T. Tetsui, K. Shindo, S. Kaji, S. Kobayashi, M. Takeyama, Intermetallics 13 (2005) 971–978.
[9] T. Tetsui, K. Shindo, S. Kaji, S. Kobayashi, M. Takeyama, Scripta Mater. 47 (2002) 399–403.
[10] D.S. Shih, Y.W. Kim, in: Niinomi, et al. (Eds.), Ti-2007 Science and Engineering [C], The Japan Institute of Metals, Kyoto, Japan, 2007, pp. 1021–1024.
[11] Y.G. Jin, J.N. Wang, Y. Wang, Scripta Mater. 51 (2004) 113–117.
[12] Y.Y. Chen, B.H. Li, F.T. Kong, J. Alloys Compd. 457 (2008) 265–269.
[13] X.J. Xu, J.P. Lin, Y. Wang, J.F. Guo, Z. Lin, G.L. Chen, J. Alloys Compd. 414 (2006) 131–136.
[14] B.J. Inkson, H. Clemens, J. Marien, Scripta Mater. 38 (1998) 1377–1382.
[15] M. Takeyama, S. Kobayashi, Intermetallics 13 (2005) 993–999.
[16] Y. Song, D.S. Xu, R. Yang, D. Li, Z.Q. Hu, Intermetallics 6 (1998) 157–165.
[17] M.A. Morris, Intermetallics 4 (1996) 417–426.
[18] F.K. Ha, Base of Fracture Physics, Science Press, Beijing, 1999.
[19] F. Appel, R. Wanger, Mater. Sci. Eng. R22 (1998) 187–268.
[20] F. Appela, M. Oehring, J.D.H. Paul, C. Klinkenberg, T. Carneiro, Intermetallics 12 (2004) 791–802.
[21] T.G. Nieh, J. Wadsworth, Mater. Sci. Eng. A239–240 (1997) 88–96.
[22] D. Vanderschueren, M. Nobuki, M. Nakamura, Scripta Metall. Mater. 28 (1993) 605–610.
[23] C.Q. Peng, B.Y. Huang, Y.H. He, J.N. Wang, Rare Met. Mater. Eng. 28 (1999) 93–96.
[24] X. Lu, X.B. He, B. Zhang, X.H. Qu, L. Zhang, Z.X. Guo, J.J. Tian, J. Alloys Compd. (2009).
[25] D.J. Duquette, N.S. Stoloff, Key Eng. Mater. 77/78 (1993) 289–299.
[26] M. Yoshihara, Y.W. Kim, Intermetallics 13 (2005) 952–958.
[27] H. Jiang, M. Hirohasi, Y. Lu, H. Imanari, Scripta Mater. 46 (2002) 639–643.
[28] M.N. Mungole, R. Balasubramaniam, A. Ghosh, Intermetallics 8 (2000) 717–720.
[29] B.G. Kim, G.M. Kim, C.J. Kim, Scripta Metall. Mater. 33 (1995) 1117–1125.
[30] T. Izumi, T. Yoshioka, S. Hayashi, T. Narita, Intermetallics 9 (2001) 547–558.
[31] Y. Wu, K. Hagihara, Y. Umakoshi, Intermetallics 12 (2004) 519–532.
[32] B.-H. Li, Study on microstructure and properties of TiAl based alloys containing yttrium, PhD dissertation [D], Harbin Institute of Technology, Harbin, China, 2007 (in Chinese).
[33] P.C. Tsai, J.H. Lee, C.S. Hsu, Surf. Coat. Technol. 201 (2007) 5143–5147.